

# Capacitances in micro-strip detectors: a conformal mapping approach

Paolo Walter Cattaneo  
Paolo.Cattaneo@pv.infn.it  
INFN Pavia, Via Bassi 6, Pavia, I-27100, Italy

---

## Abstract

The knowledge of capacitance in semiconductor micro-strip detectors is important for a correct design, simulation and understanding of the detectors.

Analytical approaches can efficiently complement numerical methods providing quick results in the design phase.

The conformal mapping method has proved to be the most effective analytical approach providing many realistic models [1]-[2].

In this paper improved analytical results are presented and compared with experimental data.

The excellent agreement between predictions and measurements confirms the relevance of this approach to modeling realistic detectors.

*Key words:* Elliptic functions, Conformal mappings, Micro-strip detectors

*PACS:* 33E05, 30C20

---

## 1. The role of capacitances in micro-strip detectors

A micro-strip detector can be modeled as a circuit: the energy release is a current generator and the resulting signal propagates in a network of capacitances and resistances. The nodes of the network are the strips and the backplane. A realistic model might incorporate also the read out electronics [2]. The capacitive elements of the circuitual model are shown in Fig.1:  $C_g$  is the strip to ground capacitance, while  $C_n$  is the interstrip capacitance  $n$  strips away.

The relation between the output signals and the energy release is mediated by the detector capacitances. These are difficult to calculate because of the complex multi-electrode geometry.

A numerical solution of the Poisson equation within the detector is possible

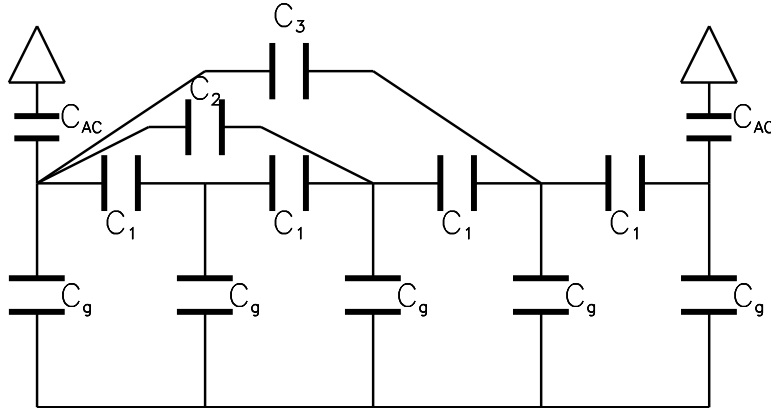


Figure 1: Capacitive circuit model of a micro-strip detector section. Every 4th strip is read out, employing the principle of capacitive charge division.

but is of limited use for the design because it has to be repeated for every configuration. Therefore it is interesting to investigate approximate analytical solutions.

## 2. Capacitance calculations with conformal mapping

### 2.1. Conformal mapping

A powerful approach to calculate electrostatic fields and capacitances in complex geometry with 2D symmetry is the use of conformal mappings [3]-[4]-[1]. They are angle preserving 1 to 1 functions between regions of the complex plane. This property is equivalent to the requirement that they are differential as complex functions [5].

An electrostatic field satisfying the Laplace equation in a region with 2D symmetry can be described by a complex potential function  $F(z = x + iy) = t(x, y) = u(x, y) + iv(x, y)$ , where  $u(x, y)$  is the potential function and  $v(x, y)$  the flux function defined such that the curves with constant  $v(x, y)$  and with constant

$u(x, y)$  are orthogonal. Both  $v(x, y)$  and  $u(x, y)$  satisfy the Laplace equation and  $F$  is differential and conformal.

Any conformal function preserves potential and flux functions and the capacitances between corresponding conductors.

This property is the key for using conformal mapping in capacitance calculation. A region with a non-trivial distribution of conductors (and/or boundary conditions) is mapped onto a region (possibly through intermediate configurations and exploiting symmetry) where the capacitance is known, e.g. parallel plates.

### 2.2. Schwartz-Christoffel transformations

The class of conformal mappings relevant for our application are the Schwartz-Christoffel transformations. They map the upper half of the complex  $t$ -plane onto the interior of a polygon in such a way that the real axis is mapped onto the boundary.

Referring to Fig.2, the mapping is

$$\frac{dz}{dt} = S(t-a)^{(\alpha/\pi)-1}(t-b)^{(\beta/\pi)-1}(t-c)^{(\gamma/\pi)-1}. \quad (1)$$

where  $S$  is a constant of scale and  $a, b, c, \dots$  are the point of the real axis corresponding to the polygon vertices.

If the polygon is a rectangle, it has four vertices and all angles equal to  $\pi/2$ . In this case Eq.1 can be written in integral form as

$$z(t) = S \int_{t_0}^t dt' (t' - a)^{-\frac{1}{2}} (t' - b)^{-\frac{1}{2}} (t' - c)^{-\frac{1}{2}} (t' - d)^{-\frac{1}{2}} \quad (2)$$

This 4 parameter class of integrals can be reduced to the following one parameter class to be discussed in the next section

$$z(t, k) = S' \int_0^t dt' [(1 - t'^2)(1 - k^2 t'^2)]^{-\frac{1}{2}} \quad (3)$$

### 2.3. Elliptic integrals and functions

A large class of integrals involving rational functions of root square of polynomials up to the fourth degree can be reduced to three types of parametrized integrals, the elliptic integrals of first, second and third kinds.

The elliptic integral of first kind in its Legendre normal form is the expression

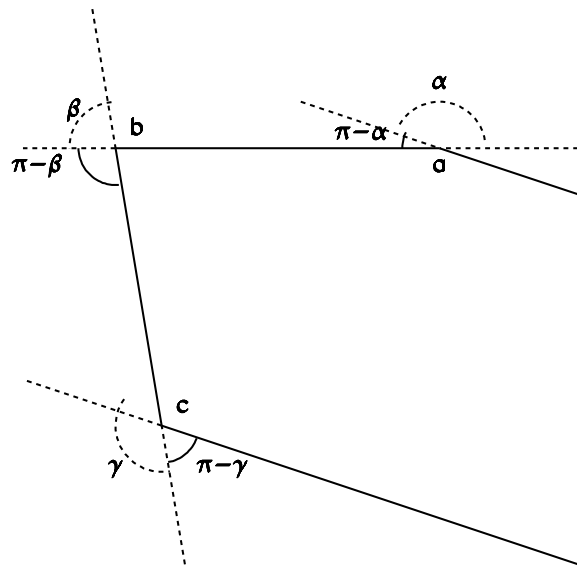


Figure 2: Example of Schwarz-Christoffel transformation

in Eq.3 with  $S' = 1$ . For a general  $t$ , the integral is said to be *incomplete* and is given the symbol  $F(t, k)$ , where  $k$  is called the *modulus*. When  $t = 1$ , it is *complete* and is given the symbol  $K(k) = F(1, k)$ . Derived from  $k$  is the *complementary modulus*,  $k' = \sqrt{1 - k^2}$ . Another definition is  $K'(k) = K(k')$ . In [6] the following important relation is derived

$$F(\pm 1/k, k) = \pm K(k) - iK(k') \quad (4)$$

Other relations deduced from the definition of  $F(t, k)$  are

$$\begin{aligned} F(t, k) - F\left(\frac{1}{k}, k\right) &= -F(1, k) + F\left(\frac{1}{kt}, k\right) \quad t \geq \frac{1}{k} \\ F(t, k) &= -iK(k') + F\left(\frac{1}{kt}, k\right) \end{aligned} \quad (5)$$

Eq.5 reduces the calculation of  $F(t, k)$  for  $t \geq \frac{1}{k}$  to the evaluation of  $F(t, k)$  for  $t \leq 1$ . In particular  $\lim_{t \rightarrow \pm\infty} F(t, k) = -iK(k')$ .

Inverting Eq.3 with  $S' = 1$ ,  $t$  is expressed as function of  $z$  and  $k$ , defining the function sine amplitude  $sn$

$$t = sn(z, k) \quad (6)$$

#### 2.4. Capacitance calculation with Schwartz-Christoffel mapping

The application of conformal mapping to capacitance calculation in geometry with 2D symmetry is based on the fact that capacitance is preserved by conformal transformations. For regions with strips and planes on the boundary, the mapping is a Schwartz-Christoffel transformation [4]-[1]-[7].

The basic configuration is shown in Fig.3, where the upper half of the  $t$ -plane is mapped into the interior of the rectangle in the  $z$ -plane.

The mapping is expressed by elliptic integrals and functions

$$z = \frac{1}{2K(k)} F\left(\frac{t}{W_t/2}, k\right) \quad k = \frac{W_t}{W_t + 2S_t} \quad (7)$$

where  $W_t$  and  $S_t$  are the strip and gap widths in the  $t$ -plane.

This function maps the strip in the  $t$ -plane onto the upper side of the rectangle in the  $z$ -plane and the two lateral half-planes onto the lower side. In the  $z$ -plane

the rectangle width is  $W_z = 1$  and the height is  $h_z = \frac{K'(k)}{2K(k)}$ .

The reverse mapping is

$$t = \frac{W_t}{2} \operatorname{sn}(2K(k)z, k) \quad (8)$$

The capacitance between the strip and the planes in the upper half of the  $t$ -plane is equal to the parallel plane capacitance in the  $z$ -plane

$$C = \epsilon \frac{W_z}{h_z} = \epsilon \frac{2K(k)}{K'(k)} \quad (9)$$

where  $\epsilon$  is the dielectric constant of the material.

If the upper and lower half-planes of the  $t$ -plane are filled with media with different dielectric constants  $\epsilon_1$  and  $\epsilon_2$ , the field component normal to the non-conducting boundaries is assumed to be zero, so that the calculation is done separately for the two half-planes.

This approach has been pioneered in [1] where several structures approximating a micro-strip detector section were studied. The major limitation in the analytical calculation using conformal transformation consisted in approximating the lateral strips as a single lateral half-plane so that  $C_n$  could not be estimated separately.

This estimation was possible using a mixed analytical-numerical method [8]-[9] that, beyond conformal transformation, involves numerical integration and matrix inversion.

In this paper this limitation is removed and the relevant capacitances are expressed by analytical expressions.

### 2.5. Auxiliary structure

The structure in Fig.4 is used in the following as an intermediate configuration and we need the capacitance of the strip to the opposite plane.

This capacitance is calculated applying two transformations. The first one maps the interior of the rectangle in the  $z$  plane onto the upper half of the  $t$ -plane

$$t = \operatorname{sn} \left( 2K(k_1) \frac{z}{W_z + S_z^l + S_z^r}, k_1 \right) \quad (10)$$

where the strip width  $W_z$  and the left and right half-gaps  $S_z^l$  and  $S_z^r$  are defined in Fig.4. The modulus  $k_1$  is defined by

$$\frac{W_z + S_z^l + S_z^r}{h_z} = 2 \frac{K(k_1)}{K'(k_1)} \quad (11)$$

This transcendental equation can be approximately, but with high precision, solved employing a series expansion from [6]. The first order is

$$\frac{K'(k)}{K(k)} = \begin{cases} \frac{1}{\pi} \ln(2 \frac{1+\sqrt{k'}}{1-\sqrt{k'}}) & 0 \leq k \leq \frac{1}{\sqrt{2}} \\ \frac{\pi}{\ln(2 \frac{1+\sqrt{k}}{1-\sqrt{k}})} & \frac{1}{\sqrt{2}} \leq k \leq 1.0 \end{cases} \quad (12)$$

that can be inverted to obtain  $k$ , defining  $y = \frac{K'(k)}{K(k)}$ , as

$$\begin{aligned} k' &= \left( \frac{\exp^{\pi y} - 2.}{\exp^{\pi y} + 2.} \right)^2 & \frac{K'(k)}{K(k)} &\geq 1 \\ k &= \left( \frac{\exp^{\pi/y} - 2.}{\exp^{\pi/y} + 2.} \right)^2 & \frac{K'(k)}{K(k)} &\leq 1 \end{aligned} \quad (13)$$

In the  $t$ -plane the strip width and the half-gaps are

$$\begin{aligned} W_t &= sn \left( 2K(k_1) \frac{S_z^l + W_z - S_z^r}{W_z + S_z^l + S_z^r}, k_1 \right) - sn \left( 2K(k_1) \frac{S_z^l - W_z - S_z^r}{W_z + S_z^l + S_z^r}, k_1 \right) \\ S_t^l &= sn \left( 2K(k_1) \frac{S_z^l - W_z - S_z^r}{W_z + S_z^l + S_z^r}, k_1 \right) + \frac{1}{k_1} \\ S_t^r &= \frac{1}{k_1} - sn \left( 2K(k_1) \frac{S_z^l + W_z - S_z^r}{S_z^l W_z + S_z^l + S_z^r}, k_1 \right) \end{aligned} \quad (14)$$

With the definitions

$$\begin{aligned} t^l &= -sn \left( 2K(k_1) \frac{S_z^l - W_z - S_z^r}{S_z^l W_z + S_z^l + S_z^r}, k_1 \right) \\ t^r &= sn \left( 2K(k_1) \frac{S_z^l + W_z - S_z^r}{S_z^l W_z + S_z^l + S_z^r}, k_1 \right) \end{aligned} \quad (15)$$

the mapping from the upper half of the  $t$ -plane to the interior of the rectangle in the  $u$ -plane is

$$u(t) = \int_0^t \frac{dt'}{\sqrt{(t' - t^l)(t' - t^r)(t' - \frac{1}{k_1})(t' + \frac{1}{k_1})}} \quad (16)$$

Following the steps outlined in [4]-[10]-[11], the capacitance is

$$C = \epsilon \frac{W_u}{h_u} = \epsilon \frac{K'(k_2)}{K(k_2)} \quad k_2 = \sqrt{\frac{S_t^l}{W_t + S_t^l}} \sqrt{\frac{S_t^r}{W_t + S_t^r}} \quad (17)$$

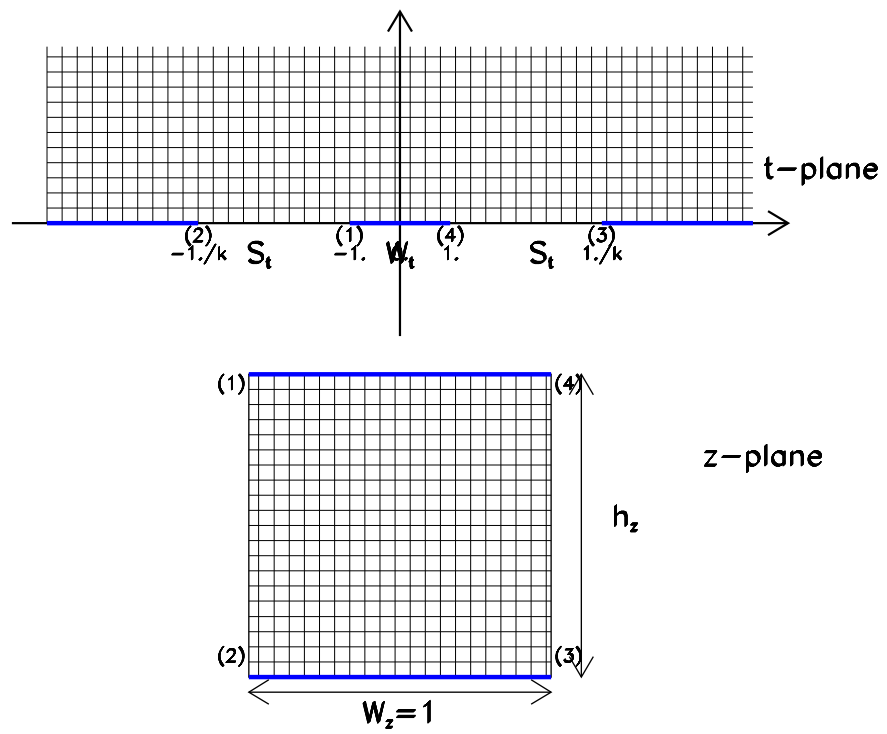


Figure 3: Mapping strip with two planes into a rectangular domain. Top: original structure, upper half-plane; bottom: parallel plane capacitor



### 3. Strip to ground capacitance

The strip to ground capacitance  $C_g$  is calculated applying the Schwartz-Christoffel mapping from the rectangular domain in the  $z$ -plane to the upper half of the  $t$ -plane and then the reverse mapping to the rectangular domain in the  $u$ -plane with a different modulus as in Fig.5.

The mapping from  $z$  plane to  $t$  plane is

$$t = sn \left( 2K(k_1) \frac{z}{W_z + S_z}, k_1 \right) \quad (18)$$

where the modulus  $k_1$  is obtained implicitly from

$$\frac{W_z + S_z}{h_z} = 2 \frac{K(k_1)}{K'(k_1)} \quad (19)$$

that can be solved using Eq.12-13.

The mapping from  $t$  plane to  $u$  plane is the elliptic integral

$$u = F \left( \frac{t}{sn \left( K(k_1) \frac{W_z}{W_z + S_z}, k_1 \right)}, k_2 \right) \quad (20)$$

where  $k_2 = k_1 sn \left( K(k_1) \frac{W_z}{W_z + S_z}, k_1 \right)$  and  $k_1$  come from Eq.19 or Eq.12.

The capacitance is

$$C_g = \epsilon \frac{W_u}{h_u} = \epsilon \frac{2K(k_2)}{K'(k_2)} \quad (21)$$

In Fig.6  $C_g$  normalized to the parallel plate capacitance  $C_{pp} = \epsilon \frac{W_z + S_z}{h_z}$  is plotted versus the  $\frac{W_z}{W_z + S_z}$  with  $\frac{W_z + S_z}{h_z}$  as parameter.

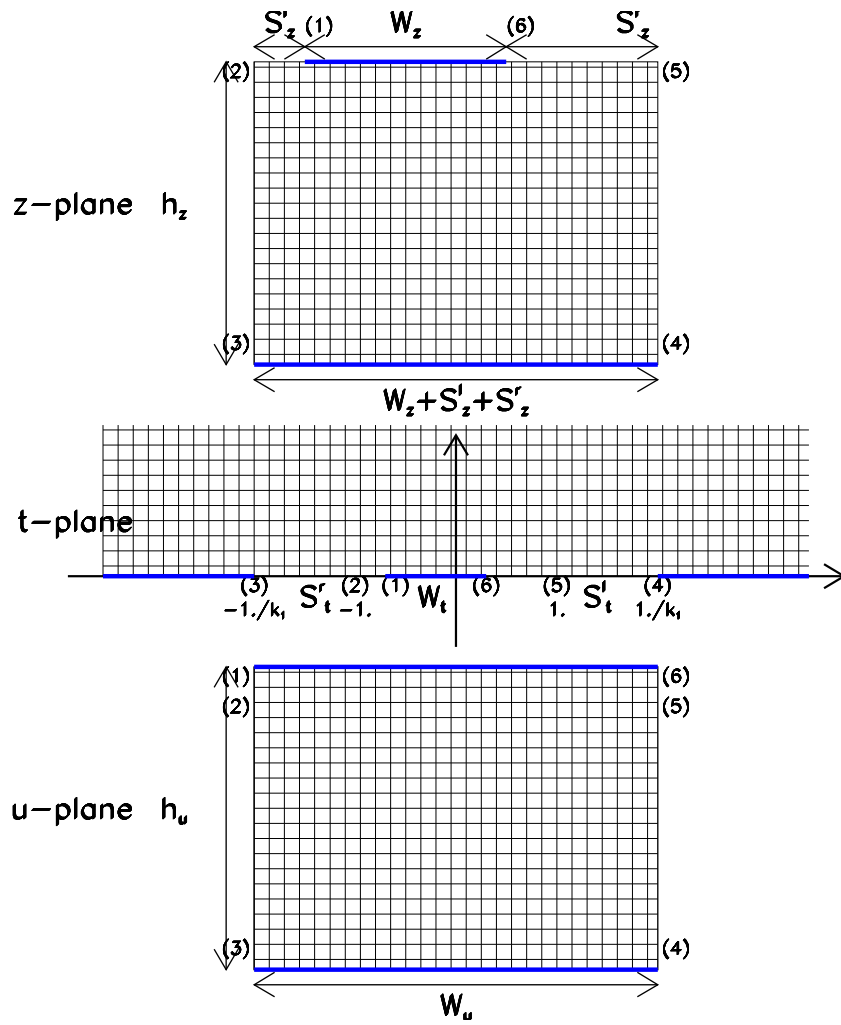


Figure 4: Mapping sequence for calculating  $C$  in a rectangle with asymmetric gaps. Top: original structure; middle: intermediate structure, upper half-plane; bottom: parallel plane capacitor

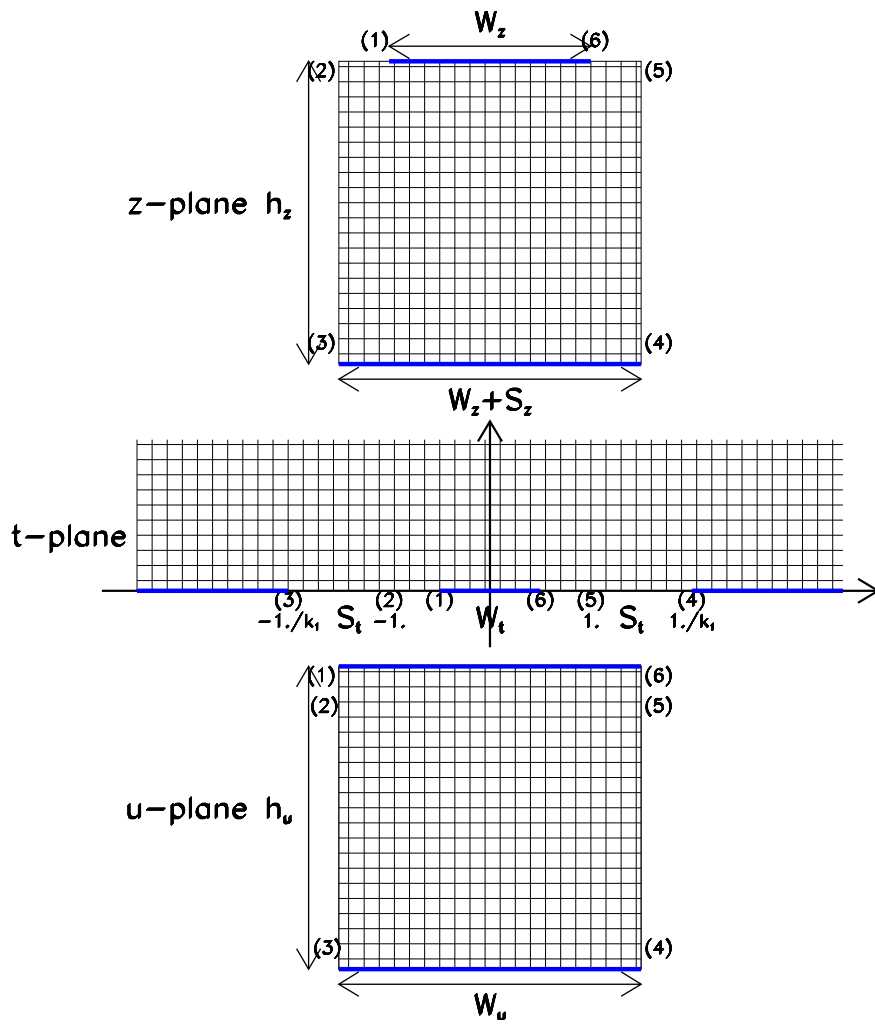


Figure 5: Mapping sequence for calculating  $C_g$ . Top: original structure; middle: intermediate structure, upper half-plane; bottom: parallel plane capacitor

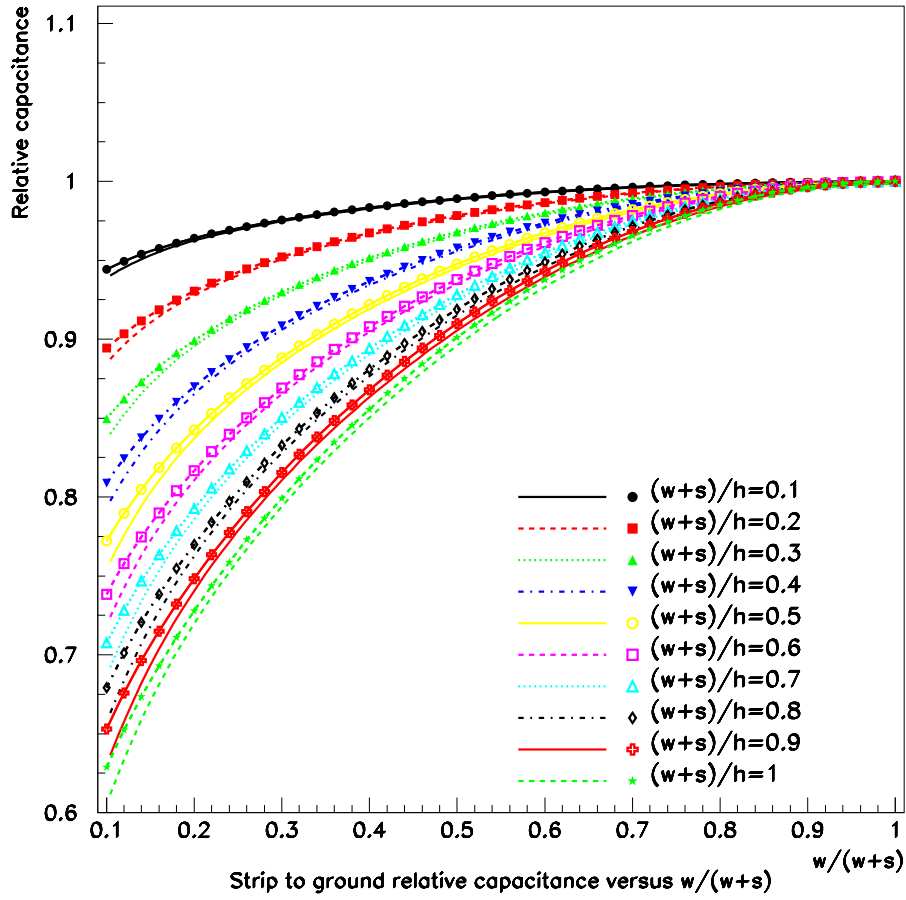


Figure 6:  $C_g$  normalized to parallel plane capacitance  $C_{pp}$  versus  $\frac{w}{w+s}$  and  $\frac{w+s}{h}$  ( $w$  is the strip width,  $s$  the interstrip gap and  $h$  the height). The curves with symbols are the results of the calculations in this paper. The curves without symbols are the results of the empirical model proposed in [12].

## 4. Interstrip capacitances

### 4.1. Preliminary considerations

The geometry of the detector relevant for the study of interstrip capacitances is displayed in Fig.7. The upper half of the  $t$  plane is in air, the lower half in the detector material, silicon in the following examples.

A simplified assumption is that the silicon section extends indefinitely, that is  $h \rightarrow \infty$ . In this case each interstrip capacitance is obtained multiplying the half-plane capacitance by  $1 + \epsilon_r^{Si}$  ( $\epsilon_r^{Si}$  is the relative silicon dielectric constant). For later use we assume that the point on each gap where the electric field generated by a voltage applied on the central strip is normal to the detector surface is in the gap center (interstrip points). These points must exist for continuity of the electric field and the field lines connecting them with the central strip divide the detector in separate regions. For each lateral strip, these regions are the volumes where a test positive charge would drift under the action of the electric field due to the central strip.

In Fig.7 the coordinates of the strip edges  $x_{in}$ ,  $x_{on}$  and the gap centers  $x_{cn}$  of a small section of the detector are labeled. The interstrip capacitances in the upper half-plane are estimated with the help of Fig.8.  $x_{cn}$  are the interstrip points.

The points marked on the picture are:

$$x_{in} = n(W_t + S_t) - W_t/2 \quad (22)$$

$$x_{on} = n(W_t + S_t) + W_t/2 \quad (23)$$

$$x_{cn} = (n + 1/2)(W_t + S_t) \quad (24)$$

The reason for introducing these interstrip points is that it can be proved that in the rectangular domain the field lines running from these points to the opposite plane are straight lines normal to the planes. Those divide the rectangular domain in smaller rectangles with the geometry shown in Fig.4 in which the Poisson equation can be solved separately.

### 4.2. Capacitances between neighbouring and not-neighbouring strips

In Fig.8 the upper half of the  $t$ -plane is mapped onto the interior of the rectangle in the  $u$ -plane by the transformation

$$u = \frac{1}{K(k_1)} F\left(\frac{t}{W_t/2}, k_1\right) \quad k_1 = \frac{W_t}{W_t + 2S_t} \quad (25)$$

The central strip in the  $t$  plane is mapped onto the upper side in the  $u$  plane with width  $W_u = 2$ . The gaps on the side of the central strip are mapped onto the lateral sides of the rectangle.

Eq.4 gives

$$h_u = K(k'_1) \quad (26)$$

and Eq.5 implies that all lateral strips are mapped onto strips on the lower side of the rectangle.

The  $n - th$  lateral strip is mapped onto a strip with width

$$\begin{aligned} W_{un} &= F(x_{on}/(W_t/2), k_1) - F(x_{in}/(W_t/2), k_1) \\ &= F\left(-\frac{1}{k_1} + (2n+1)\frac{W_t + S_t}{W_t}, k_1\right) - F\left(\frac{1}{k_1} + (2n-1)\frac{W_t + S_t}{W_t}, k_1\right) \end{aligned} \quad (27)$$

The left and right gaps of the  $n - th$  lateral strip are mapped onto gaps with widths (defining  $n = 1$   $F(x_{cn-1}/(W_t/2), k_1) = 0$ )

$$\begin{aligned} S_{un}^l &= F(x_{cn}/(W_t/2), k_1) - F(x_{on}/(W_t/2), k_1) \\ &= F\left((2n+1)\frac{W_t + S_t}{W_t}, k_1\right) - F\left(-\frac{1}{k_1} + (2n+1)\frac{W_t + S_t}{W_t}, k_1\right) \end{aligned} \quad (28)$$

$$\begin{aligned} S_{un}^r &= F(x_{in}/(W_t/2), k_1) - F(x_{cn-1}/(W_t/2), k_1) \\ &= F\left(\frac{1}{k_1} + (2n-1)\frac{W_t + S_t}{W_t}, k_1\right) - F\left((2n+1)\frac{W_t + S_t}{W_t}, k_1\right) \end{aligned} \quad (29)$$

The problem of calculating  $C_n$  in a half-plane is reduced to the calculation of the strip to backplane capacitance in a structure like Fig.4, following the steps described previously. The contributions in air and in silicon are added.

The steps are the following: a modulus  $k_1$  is determined by

$$\frac{W_{un} + S_{un}^l + S_{un}^r}{h_u} = 2\frac{K(k_1)}{K'(k_1)} \quad (30)$$

using Eq.12. Eq.14 gives

$$W_n = sn\left(2K(k_1)\frac{S_{un}^l + W_{un} - S_{un}^r}{W_{un} + S_{un}^l + S_{un}^r}, k_1\right) - sn\left(2K(k_1)\frac{S_{un}^l - W_{un} - S_{un}^r}{W_{un} + S_{un}^l + S_{un}^r}, k_1\right)$$

$$S_n^l = sn \left( 2K(k_1) \frac{S_{un}^l - W_{un} - S_{un}^r}{W_{un} + S_{un}^l + S_{un}^r}, k_1 \right) + \frac{1}{k_1} \quad (32)$$

$$S_n^r = \frac{1}{k_1} - sn \left( 2K(k_1) \frac{S_{un}^l + W_{un} - S_{un}^r}{S_{un}^l W_{un} + S_{un}^l + S_{un}^r}, k_1 \right) \quad (33)$$

$$(34)$$

and therefore the  $n$ -th order interstrip capacitance is

$$C_n = \epsilon \frac{2K(k_2^n)}{K'(k_2^n)} \quad k_2^n = \sqrt{\frac{S_n^l}{W_n + S_n^l}} \sqrt{\frac{S_n^r}{W_n + S_n^r}} \quad (35)$$

The interstrip capacitance  $C_1$  between neighboring strips is displayed in Fig.9 versus  $W/(W + S)$ . The higher order interstrip capacitances  $C_n$  for  $n \in (2, 7)$  are displayed in Fig.10.  $C_1$  depends strongly on  $W/(W + S)$  while the  $C_n$  dependence is much weaker.

Fig.11 displays the total interstrip capacitance  $C_{is,tot}$  obtained adding all interstrip capacitances up to the 7-th order on both sides and the total capacitance  $C_{tot} = C_{is,tot} + C_g$ . These quantities are easier to measure than  $C_n$  and to compare with experimental data.

## 5. Comparison with other approaches and experimental results

The results presented so far refer to geometrical capacitances in fully depleted detectors with strips on the junction side. Realistic detectors may differ from this model for various reasons. The most relevant is the presence of free charges below the interstrip oxide acting as additional conducting layers. This effect is difficult to predict and describe and may alter significantly the measurements.

For detectors not satisfying the previous conditions, either our model is made more realistic, and more difficult to solve analytically, or a numerical approach

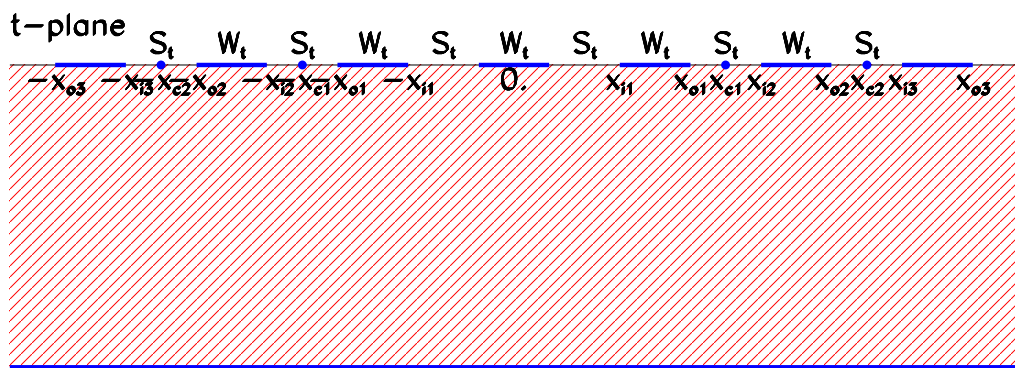


Figure 7: Section of a micro-strip detector with strip edges and interstrip gap centers marked.



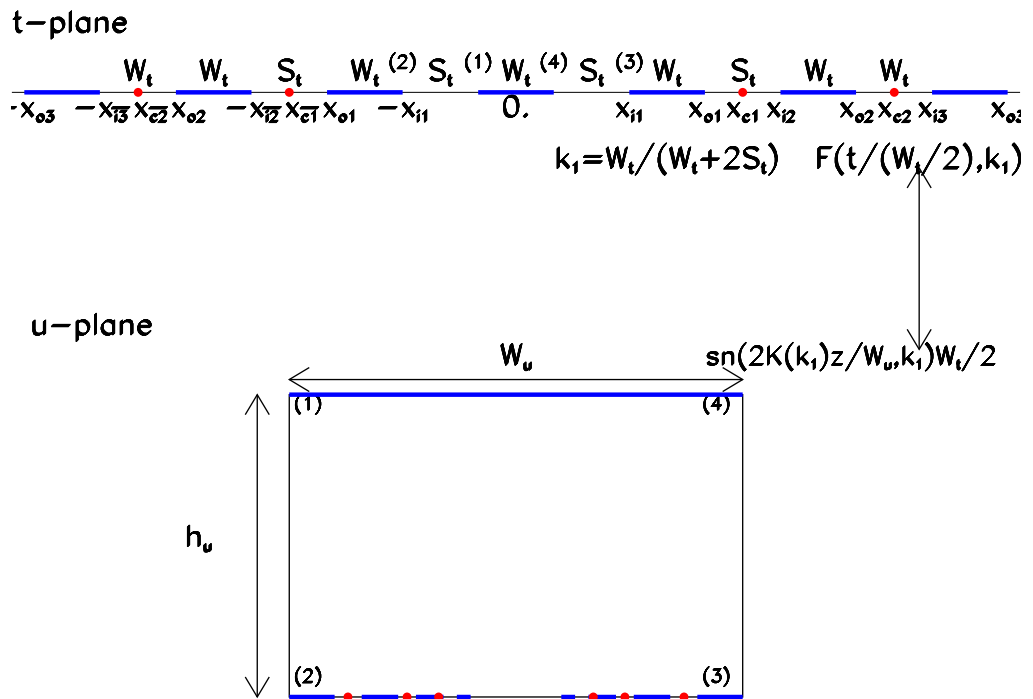


Figure 8: Mapping of the half-plane in air. Top: original structure with few strips, the strips extends indefinitely on both sides. Bottom: rectangular domain with all lateral strips mapped on the lower side.

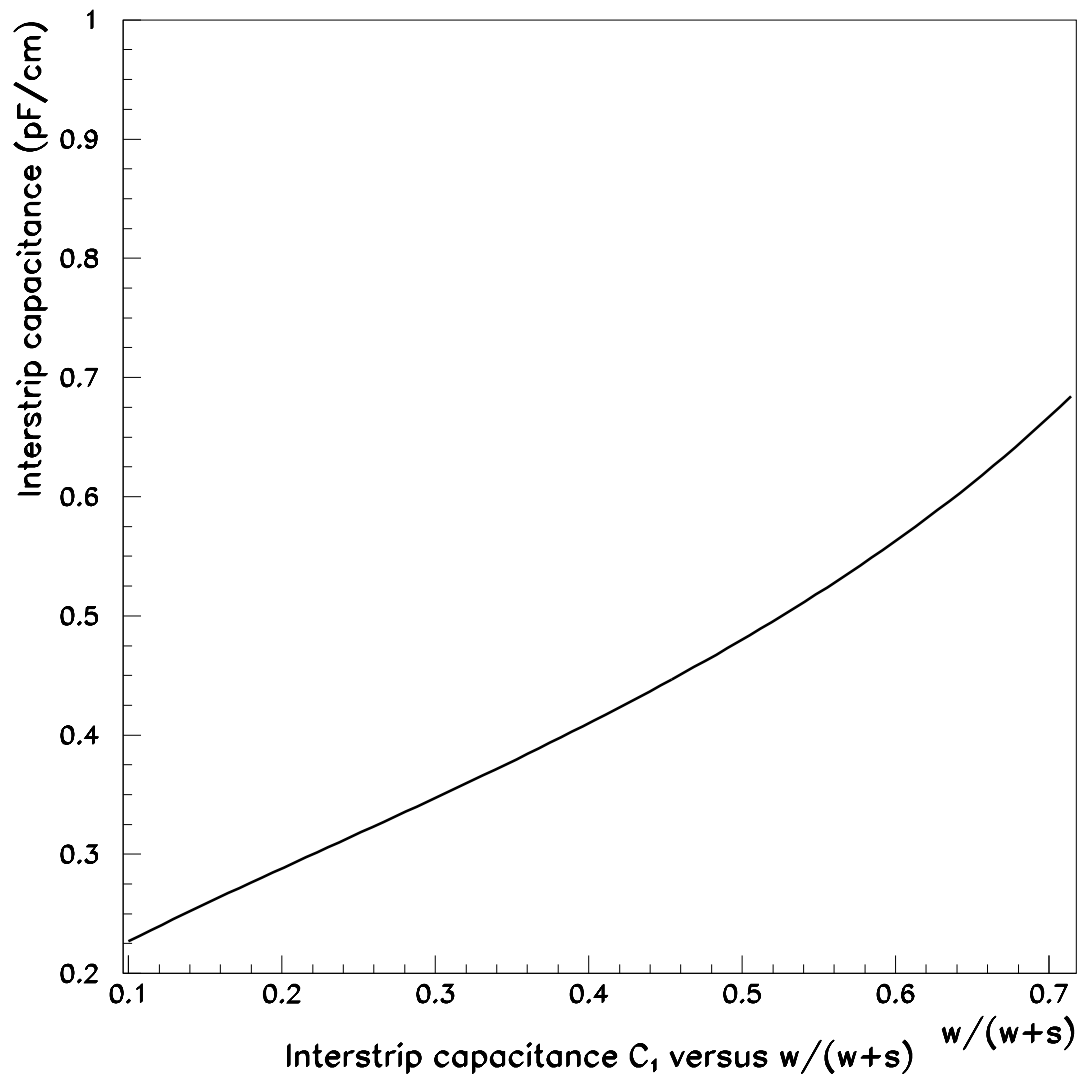


Figure 9: Plot of the first order interstrip capacitance  $C_1$  versus  $w/(w + s)$  ( $w$  is the strip width,  $s$  the interstrip gap and  $h$  the height).

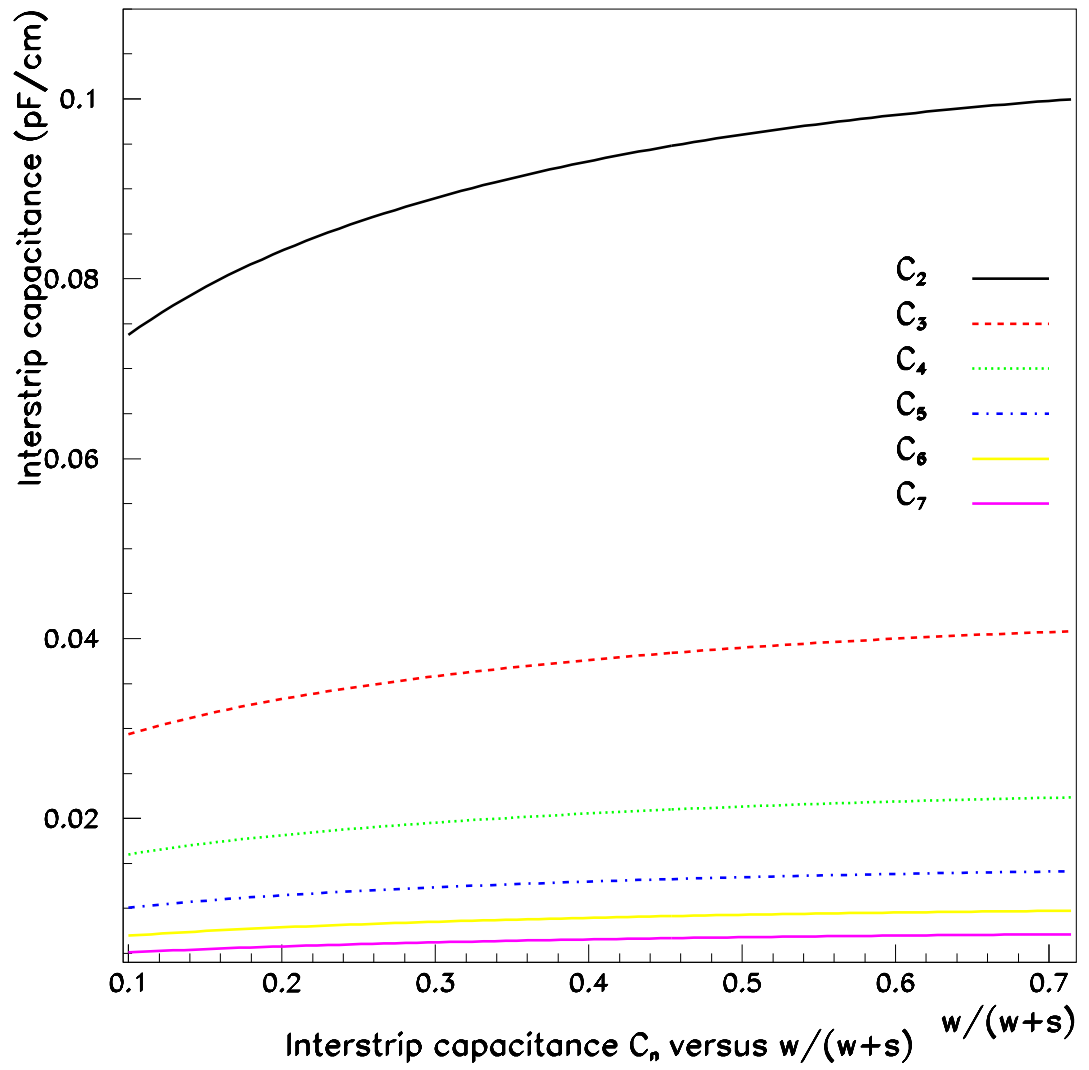


Figure 10: Plot of the higher order interstrip capacitances  $C_n$  versus  $w/(w+s)$  ( $w$  is the strip width,  $s$  the interstrip gap and  $h$  the height).

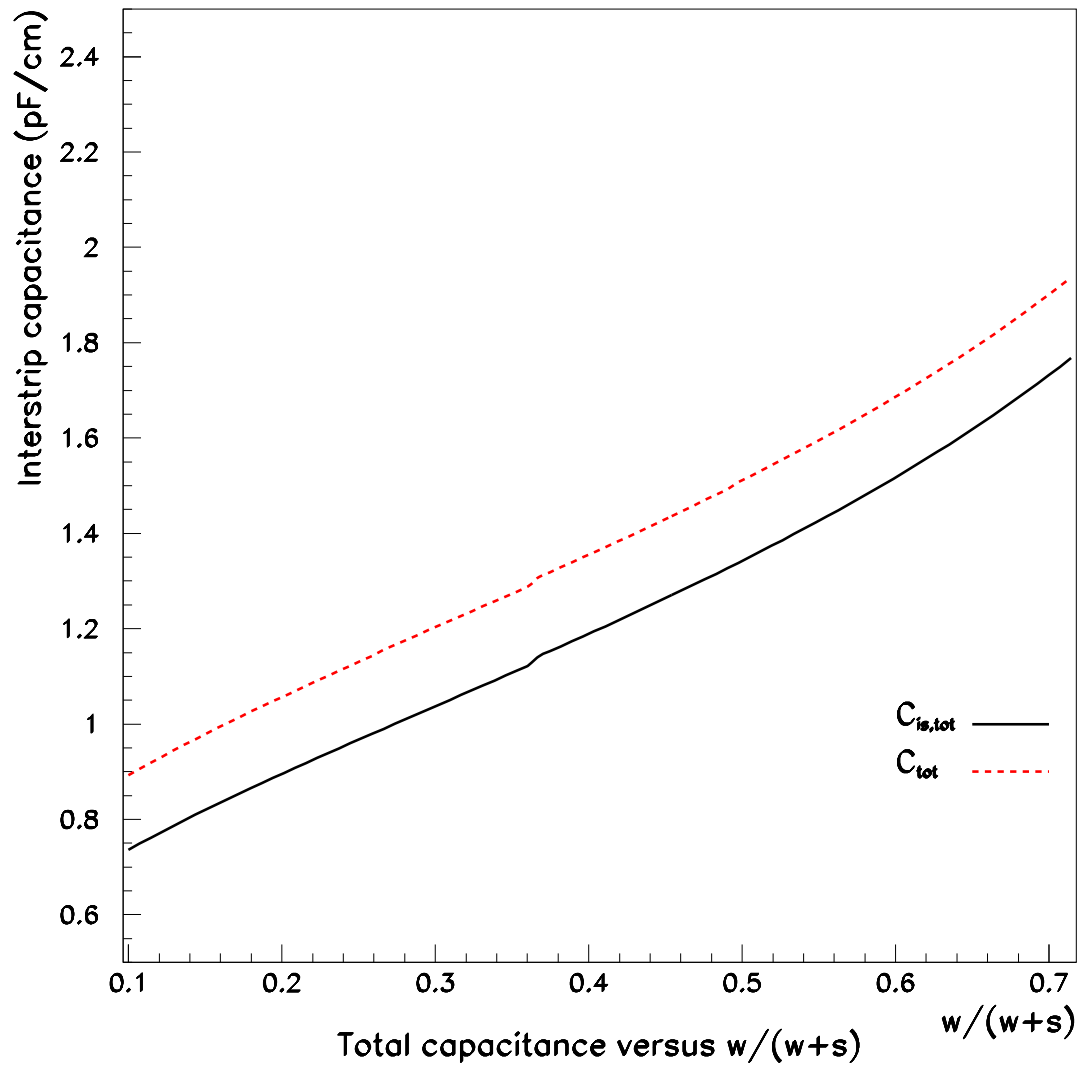


Figure 11: Plot of the total interstrip  $C_{is,tot}$  and total  $C_{tot}$  capacitances versus  $w/(w+s)$  for  $w+s=50\mu\text{m}$  and  $h=300\mu\text{m}$ . ( $w$  is the strip width,  $s$  the interstrip gap and  $h$  the height).

like that in [13] can complement our analytical approach by studying the effects of deviation from ideality.

In the following, the field of applicability of the calculations developed in this paper is studied by comparing them with other models and the experimental results presented in [12, 14]. These results have been selected because they refer to fully depleted detectors with strips on the junction side and scan a broad range of detector parameters. Furthermore data are presented in a format adequate for comparison with calculations.

### 5.1. $C_g$ comparison

In Fig.6 the values of  $C_g$  calculated with our model are compared with the empirical formula developed in [12] obtained fitting the results of the numerical solution of the Poisson equation presented in [15]. This formula is expressed as

$$\frac{C_g}{C_{pp}} = \frac{1}{1 + \frac{W+S}{h} f\left(\frac{W}{W+S}\right)} \quad (36)$$

where  $f\left(\frac{W}{W+S}\right)$  is defined in [12]. This model is supported by experimental results presented in [12, 14].

In [14] results for different material orientations  $\langle 111 \rangle$  and  $\langle 100 \rangle$  are presented.  $\langle 111 \rangle$  has an higher trapped charge at the Si-O<sub>2</sub> interface and is more sensitive to irradiation. Nevertheless for nonirradiated devices, in the frequency range relevant for detector signal and for adequately high overdepletion voltage the capacitances are not dependent on the material orientation but only on the detector geometry and can be compared to our calculations.

Fig.6 shows an excellent agreement between our results and Eq.36. Therefore, at least for  $C_g$ , detectors can be operated in such a condition that the geometrical capacitances are experimentally measurable and they are described very well by our calculations.

### 5.2. $C_n$ comparison

A comparison of  $C_n$  is possible with the model developed in [1], where the  $C_n$  for  $n \in (2, 7)$  were calculated for  $W = S$ . The results are compared in Tab.1 showing an excellent agreement

Measuring separately  $C_n$  is quite difficult. The most straightforward comparison is with the total capacitance  $C_{tot}$  (including  $C_g$ ) or with the total interstrip capacitance  $C_{is,tot}$ .

Table 1:  $C_n$ (fF/cm) calculated in [1] and in this paper for  $W = S$

	$C_1$	$C_2$	$C_3$	$C_4$	$C_5$	$C_6$	$C_7$
[1]	487.	96.	40.	22.	13.	9.	6.
Eq.35	478.	95.	39.	21.	13.	9.	7.

### 5.3. $C_{tot}$ comparison

Experimental measurements of  $C_{tot}$  are presented in [12, 14]. In order to compare the results, it is necessary to fix also  $(W + S)/h$ .  $C_{tot}$  and  $C_{is,tot}$  shown in Fig.11 are calculated with  $W + S = 50\mu m$  and  $h = 300\mu m$ . The easiest comparison is with the formula, supported by measurements on fully depleted detectors with strips on the junction side, presented in [14],

$$C_{tot} = 0.8 + 1.6 \frac{w}{w+s} pF/cm \quad (37)$$

A linear fit to  $C_{tot}$  in Fig.11 (not shown) gives

$$C_{tot} = 0.73 + 1.60 \frac{w}{w+s} pF/cm \quad (38)$$

showing an excellent agreement.

## 6. Conclusions

The capacitances in micro-strip detectors are calculated analytically with the help of Schwartz-Christoffel conformal transformations. The results are expressed with elliptic functions.

The strip to ground, the total and the interstrip capacitances are calculated as function of the geometry of the detector.

The results are compared with other models and with empirical formulae supported by experimental measurements showing an excellent agreement for non-irradiated and fully depleted detectors.

## Appendix

The numerical evaluation of the complete and incomplete elliptic integrals and of the elliptic functions is based on FORTRAN 77 routines from the CERN library package available in [16]. These routines are based on numerical algorithms developed in [17, 18, 19, 20].

## References

- [1] P. W. Cattaneo. Capacitance calculation in a microstrip detector and its application to signal processing. *Nucl. Instr. and Meth. A*, 295:207, 1990.
- [2] P. W. Cattaneo. Noise and signal processing in a microstrip detector with a time variant readout system. *Nucl. Instr. and Meth. A*, 359:551, 1995.
- [3] K. J. Binns and P. J. Lawrenson. *Analysis and Computation of Electric and Magnetic Field Problems*. Pergamon, Oxford, 1963.
- [4] R. Schinziger and P. A. A. Laura. *Conformal Mapping: Methods and Applications*. Elsevier, Amsterdam, 1991.
- [5] L. Alfhors. *Complex analysis*. McGraw-Hill, Singapore, 1979.
- [6] F. Oberhettinger and W. Magnus. *Anwendung der Elliptische Funktionen in Physik und Technik*. Springer, Berlin, 1949.
- [7] K. J. Binns, P. J. Lawrenson, and C. W. Trowbridge. *The analytical and numerical solution of electric and magnetic fields*. Wiley, Chichester, England, 1992.
- [8] D. Homentcovschi, A. Manolescu, A. Manuela, and C. Burileanu. A general approach to analysis of distributed resistive structures. *IEEE Transactions on Electron Device*, ED-25:787, 1987.
- [9] D. Homentcovschi, A. Manolescu, A. Manuela, and L. Kreindler. An analytical solution for the coupled stripline-like microstrip line problem. *IEEE Transactions on Microwave Theory and Technology*, MTT-36:1003, 1988.
- [10] G. Ghione and C. Naldi. Parameters of coplanar waveguides with lower ground plane, 1983.
- [11] G. Ghione and C. Naldi. Coplanar waveguides for MMIC applications: Effect of upper shielding, conductor backing, finite-extent ground planes, and line-to-line coupling. *IEEE Transactions on Microwave Theory and Technology*, MTT-29:260, 1987.
- [12] E. Barberis et al. Capacitances in silicon microstrip detectors. *Nucl. Instr. and Meth. A*, 342:90, 1994.

- [13] S. Chatterji et al. Analysis of interstrip capacitance of si microstrip detector using simulation approach. *Solid State Electronics*, 47:1491, 2003.
- [14] S. Albergo et al. Comparative study of  $\langle 111 \rangle$  and  $\langle 100 \rangle$  crystals and capacitance measurements on Si strip detectors in CMS. *Il Nuovo Cimento*, 112A(11):1261, 1999.
- [15] R. Sonnenblick et al. Electrostatic simulations for the design of silicon strip detectors and front-end electronics. *Nucl. Instr. and Meth. A*, 310:189, 1991.
- [16] *CERNLIB Short Writeups*, 1996.
- [17] R. Bulirsch. Numerical calculations of elliptic integrals and elliptic functions. *Numerische Mathematik*, 7:78–90, 1965.
- [18] R. Bulirsch. Numerical calculations of elliptic integrals and elliptic functions II. *Numerische Mathematik*, 7:353–354, 1965.
- [19] R. Bulirsch. Numerical calculations of elliptic integrals and elliptic functions III. *Numerische Mathematik*, 13:305–315, 1969.
- [20] W. J. Cody. Chebyshev approximations for the complete elliptic integrals K and E. *Mathematics of Computation*, 19:105–112, 1965.